ADVANCED FUNCTIONAL MATERIALS
www.afm-journal.de

Synergistic Computational-Experimental Approach to Improve Ionene Polymer-Based Functional Hydrogels

Jürgen Bachl, David Zanuy, Daniel E. López-Pérez, Guillermo Revilla-López, Carlos Cativiela, Carlos Alemán, and David Díaz Díaz**

Dedicated to Prof. V. Martín García on the occasion of his 60 birthday

The manifold applications of ionene-based materials such as hydrogels in daily life, biomedical sciences, and industrial processes are a consequence of their unique physical and chemical properties, which are governed by a judicious balance between multiple non-covalent interactions. However, one of the most critical aspects identified for a broader use of different polyelectrolytes is the need of raising their gelation efficiency. This work focuses on surfactant-free ionene polymers 1–3 containing DABCO and *N*,*N*′-(*x*-phenylene)dibenzamide (*x* = *ortho*-/*meta*-/*para*-) linkages as model systems to develop a combined computational-experimental approach to improve the hydrogelation through a better understanding of the gelation mechanism. Molecular dynamics simulations of isomeric ionenes 1–3 with explicit water molecules point out remarkable differences in the assembly of the polymeric chains in each case. Interchain regions with high degree of hydration (i.e., polymer···water interactions) and zones dominated by polymer···polymer interactions are evident in the case of *ortho*- (1) and *meta*- (2) isomeric ionenes, whereas domains controlled by polymer···polymer interactions are practically inexistent in 3. In excellent agreement, *ortho*-ionene 1 provides experimentally the best hydrogels with unique features such as thixotropic behavior and dispersion ability for single-walles carbon nanotubes.

1. Introduction

Polyelectrolytes are of fundamental and practical importance since many of them play critical biological functions in nature.[1–3] Within this type of macromolecules, synthetic ionenes represent an important subgroup in which the ionic groups form part of the polymer backbone.[4–10] In general, the term refers to polycations carrying quaternary ammonium as the charged species. From a synthetic point of view, ionenes are typically accessible either by 1) chain or step polymerization of suitable monomers (e.g., Menshutkin reaction between bis-tertiary amines and activated dihalides, self-polyaddition of aminoalkylhalides) or 2) cationic functionalization of reactive precursor polymers.[11,12] Since the first synthesis of an ionene more than 80 years ago by Marvel and co-workers,[13,14] they have been the subject of intensive investigations in diverse fields including chemistry, biology, physics, medicine and materials science. Such tremendous research activity has culminated with the development of manifold applications of these macromolecular materials in daily life, biosciences and industrial processes (e.g., as antibacterial agents or building blocks for the preparation of chromatography stationary phases, symplexes or functional gels, among other uses).[4]

The unique physical and chemical properties of these polymers are the result of a judicious balance between multiple interactions including hydrophobic, charge transfer and long-ranged electrostatic interactions. As for all polycations, besides the density and charge distribution along the backbone, the nature of the counterion, the molecular weight, flexibility and H-bonding capability of the polymer chain are also critical aspects that may markedly influence the conformation and dynamics of polymer chains. Additionally, their considerable structural versatility (e.g., achievable via counterion exchange, chemical modification of monomers, polymerization method) and key features such as electrostatic stabilization of colloids and tunability of their mechanical properties can be used to induce the formation of stable polyelectrolyte hydrogels for applications in biomedicine, engineering and food science.[15,16] Yet one of the critical technical issues identified for the practical use of a broader range of organic polyelectrolytes is the necessity of increasing the efficiency of gelation.[17] However, despite numerous efforts to establish structure-property relationships, the understanding of the gelation mechanism of such complex systems remains a major challenge. This is mainly due to

J. Bachl, Prof. D. D. Díaz
Institut für Organische Chemie
Fakultät für Chemie und Pharmazie
Universität Regensburg
Universitätsstr. 31, 93053 Regensburg, Germany
E-mail: david.diaz@chemie.uni-regensburg.de
Dr. D. Zanuy, D. E. López-Pérez, Dr. G. Revilla-López, Prof. C. Alemán
Departament d'Enginyeria Química
ETSEIB, Universitat Politècnica de Catalunya
Av. Diagonal 647, 08028 Barcelona, Spain
E-mail: carlos.aleman@upc.edu
Prof. C. Cativiela
Instituto de Síntesis Química y Catálisis Homogénea-ISQCH
CSIC-Universidad de Zaragoza
50009 Zaragoza, Spain
Prof. D. D. Díaz
IQAC-CSIC, Jordi Girona 18–26, 08034 Barcelona, Spain

DOI: 10.1002/adfm.201304230

1) non-uniform distribution of ionic groups along the polymer chain,[18,19] and 2) the fact that several experimental results are typically poorly described from a microscopic point of view, which makes difficult the prediction of gelation properties through simple theoretical models and the rational design of more efficient gelling agents. In this sense, conversely to other polyelectrolytes, ionenes constitute ideal systems to study ionic aggregation phenomena since the ionic sites are precisely situated along the macromolecular unit.

On the other hand, theoretical description of polyelectrolyte hydrogels at the atomistic level is very challenging because of the conformational complexity of polymer chains, which increases with the number of degrees of freedom in repeat units, the description of excluded volume interactions involved in these hydrophilic polymeric networks containing large amounts of water, and the huge dimensions of the systems necessary to represent these water-swollen ionic aggregates.[20] Thus, in spite of the interest in polyelectrolyte hydrogels, the intrinsic complexity of gelated systems and the significant amount of computational resources needed to describe their chemical details and physical properties, have severely restricted their atomistic modeling. However, in the last few years, computational advances (i.e., parallel computer architectures and efficient scalability of computer programs) have allowed the study of some of the most important polymeric hydrogels.[21–25] Because of these recent advances, approaches combining computer simulations and experimental methodologies are currently expected to be successful in the rational design of hydrogels with advanced properties.

Herein, we reasoned that using different structural isomers of phenylenediamine as molecular core for the construction of ionene polymers would lead to different types of cross-linked networks in water and, hence, potential superior hydrogels. We demonstrate that a combined computational-experimental approach can be used to rationally design more efficient ionene hydrogelators in terms of gelation kinetics as well as mechanical and functional properties of the resulting hydrogels.

2. Results and Discussion

Hydrogels based on surfactant-free linear ionenes having *N*,*N*′-(-*para*-phenylene)dibenzamide linkages were first described by Yoshida and co-workers.[26] Motivated by the remarkable properties and potential applications shown by these systems, we envisioned the possibility to develop a combined computational-experimental paradigm with the aim of enhancing the gelation efficiency of these valuable functional materials. Among the number of tertiary diamines that can be used as spacers for building the ionenes we focused for this work on 1,4-diazabicyclo[2.2.2]octane (DABCO), as this moiety has also proven useful in the development of polycations for other applications such as template synthesis of porous nanomaterials[27] and gene delivery.[28]

Our approach takes advantage of the structural isomerism of the phenylenediamine core (**Figure 1**). Depending on the substitution pattern of the phenyl ring, it is possible to grow the two polymeric arms of the ionene forming different angles to each other (i.e., $\theta = 60°$, 120°, or 180°). Such well-defined topological

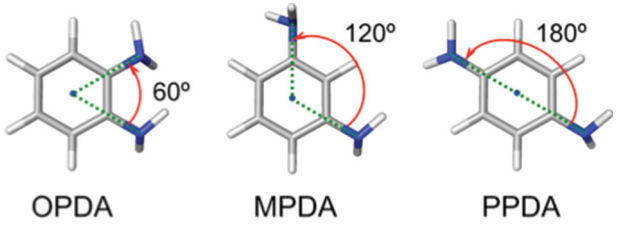

Figure 1. Phenyl ring substitution angles in phenylenediamine structural isomers: OPDA = *ortho*-phenylenediamine; MPDA = *meta*-phenylenediamine; PPDA = *para*-phenylenediamine. Different net dipole moments derive from vector addition of the moments of the respective monosubstituted compounds.

variations not only impact the net dipole moment of the polymers but also their inter- and intramolecular interactions, which are expected to influence significantly the gelation phenomenon. Thus, information provided by advanced computational modeling of these interactions at the atomistic level combined with experimental parameters of the ionenes could serve as a versatile and accurate tool to predict their hydrogelation ability.

2.1. Synthesis and Characterization of Ionenes

Following the general procedure reported by Yoshida and co-workers, the ionenes **1**–**3** (**Figure 2**) were rapidly synthesized via a two-step reaction sequence. Briefly, amidation of isomeric phenylenediamines OPDA, MPDA and PPDA with 4-(chloromethyl)benzoyl chloride in the presence of Et_3N in CH_2Cl_2 afforded the corresponding bis-benzamides (dielectrophilic monomers) in good yields (87–96%) upon recrystallization (Scheme S1, Supporting Information). Their subsequent

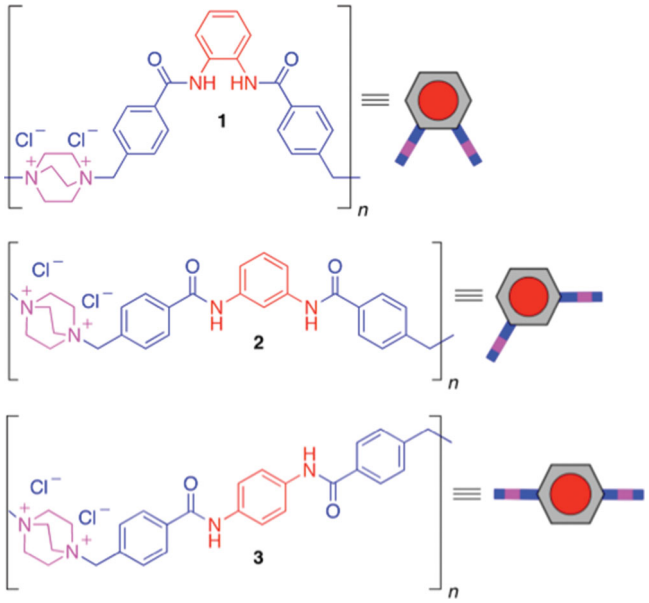

Figure 2. Synthesized DABCO-containing ionene polymers **1**–**3** with *N*,*N*′-(*x*-phenylene)dibenzamide linkages (*x* = *ortho*-/*meta*-/*para*-). A symbolic representation of each ionene is given for ease of reading and interpretation.

step-growth copolymerization with DABCO (dinucleophilic monomer) under equimolar conditions in DMF at 80 °C gave the desired polycations **1**–**3** as precipitates within 2–3 days in good yields (69–98%) after a simple filtration, washing and drying protocol (ESI).

Fundamental structural analyses of ionenes **1**–**3** were carried out by NMR, FT-IR, elemental analysis, SEC, TGA, and DSC measurements (Figures S1–S7, Supporting Information). ^{1}H-NMR spectra in D_2O clearly distinguished the expected three sets of broad resonances for each pure polymer corresponding to aromatic protons ($\delta \approx$ 7.1–8.0 ppm), benzylic methylene protons ($\delta \approx$ 4.1–4.7 ppm), and methylene protons bonded to quaternized nitrogen atoms ($\delta \approx$ 2.9–3.9 ppm). In agreement, FT-IR measurements exhibited broadening of the bands centered at ≈ 1650 cm^{-1} (C = O stretching, amide I) and 3310 cm^{-1} (N–H stretching) in comparison to precursor monomers, and new resonance features at ≈ 980–1130 cm^{-1} associated to C–N$^+$ stretching vibration. In order to achieve adequate solubility and mobility of the polymers for GPC/SEC measurements (thus, avoiding undesired polymer-column interactions), counteranion exchange of chloride by bis(trifluoromethanesulfonyl)amide (TFSA) anions was carried out using LiTFSA in hot water.[29] The results for our polymer batches showed dispersity values ($Đ = M_w/M_n$) ranged from 2.1 to 2.9, which is expected for ionenes made via step-growth polymerizations and fairly consistent with previous data.[26] In principle, the differences in the observed average molecular weights for a given batch of ionenes (i.e., 8.1 × 10^3 Da for **1**·TFSA; 1.2 × 10^4 Da for **2**·TFSA; 1.7 × 10^4 Da for **3**·TFSA, with degrees of polymerization $n \leq 10$), could have a certain impact on the thermal, mechanical and/or gelation properties (vide infra). Moreover, the lack of optical birefringence domains under crossed nicols reflected the isotropic nature of the solid polymers. Simultaneous TGA–DSC analysis of the three ionenes revealed similar thermal stability with a series of events associated to 1) endothermic moisture/solvent loss (weight loss ≈ 5–7%, $T \approx$ 78–80 °C) and 2) multi-step thermal degradation of the polymers. In general, the primary degradation pathway of these high charge density polymers begins at temperatures around 200–250 °C, which correspond to the dequaternization (Hofmann elimination) of backbone nitrogens.[30] Specifically, the starting degradation temperature for **1**, **2**, and **3** was estimated from the first endothermic transition in the DSC traces after solvent loss at ≈ 234 for **1** and 254–255 °C for **2**–**3**. In concordance with the SEC results, the higher starting decomposition temperature observed for **2** and **3** is attributed to their higher molecular weight (hence, a higher content of quaternized nitrogen groups) in comparison to **1**. These results point out the hygroscopic and amorphous nature of the polymers, as well as a relative indirect influence of the core topology on the thermal stability due to the different degree of polymerization obtained using OPDA, MPDA or PPDA. In this sense, the ionic aggregation is more prevalent when the molecular weight is higher, and hence more thermal energy is needed to dissociate the aggregates.

2.2. Computational Studies

With the aim of using computer simulations as a predictive tool for the hydrogelation of isomeric ionenes, we performed atomistic molecular dynamics (MD) simulations of **1**–**3** using molecular models formed by two polymer chains with $n = 6$ immersed in a simulation box filled with explicit water molecules. Initially, two identical ionene polymer molecules were placed at a distance of approximately 9 Å. **Figure 3** provides representative snapshots of the simulated systems during the production trajectory (i.e., after thermalization and density relaxation). Apparently the assembly between the two chains of **1** and **2** is different than that of **3**. Thus, although both **1** and **2** show regions between the two chains with a high degree of hydration, zones dominated by polymer···polymer interactions are also evident. In contrast, polymer···water are practically the only intermolecular interactions in **3**, polymer···polymer interactions being very scarce (i.e., domains controlled by polymer···polymer are practically inexistent).

These observations are corroborated in **Figure 4**a, which displays the radial distribution function for pairs of carbon atoms belonging to different chains, $g_{C\text{-}C}(r)$. Thus, the shape of the $g_{C\text{-}C}(r)$ profile is largely influenced by the molecular architecture of the ionene polymers. **2** shows a very high and well defined peak centered at 4.2 Å reflecting that intermolecular interactions between two polymer molecules are relatively strong. This peak is less intense but still prominent in **1**, remaining centered at 4.2 Å, which is consistent with a slight reduction in the strength of polymer···polymer interactions with respect to **2**. However, **1** shows other well defined peaks centered at 6.2 and 9.7 Å and a shoulder at 8.2 Å, which are not detected in **2**, suggesting that the assembly formed by the two polymer chains is very stable. In contrast, **3** only shows a broad shoulder centered at 5.2 Å suggesting that interactions between the two ionene chains are very weak, or even practically inexistent.

Similar conclusions are reached by analyzing the existence of intermolecular polymer···polymer hydrogen bonding and

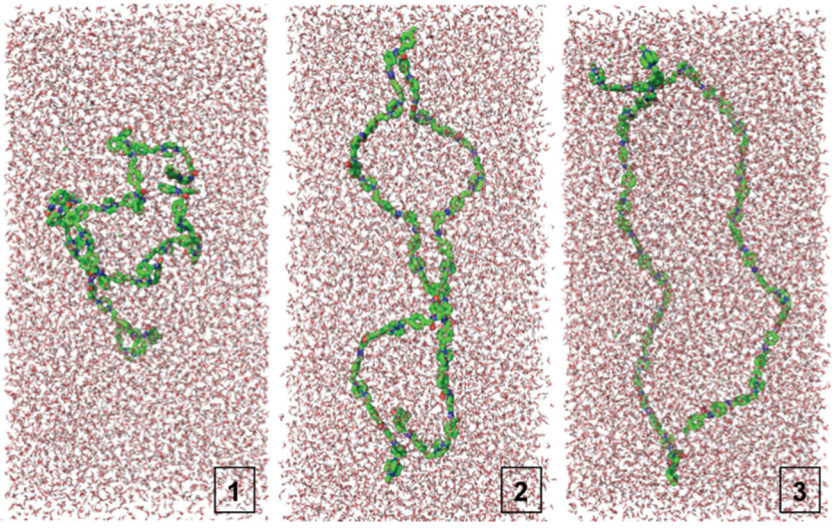

Figure 3. Representative snapshots of the three simulated systems. The numbers refer to the ionene polymer in each case. For each case, only the central zone of the simulation box, which contains the polymer chains, is displayed while the rest has been omitted for the clarity.

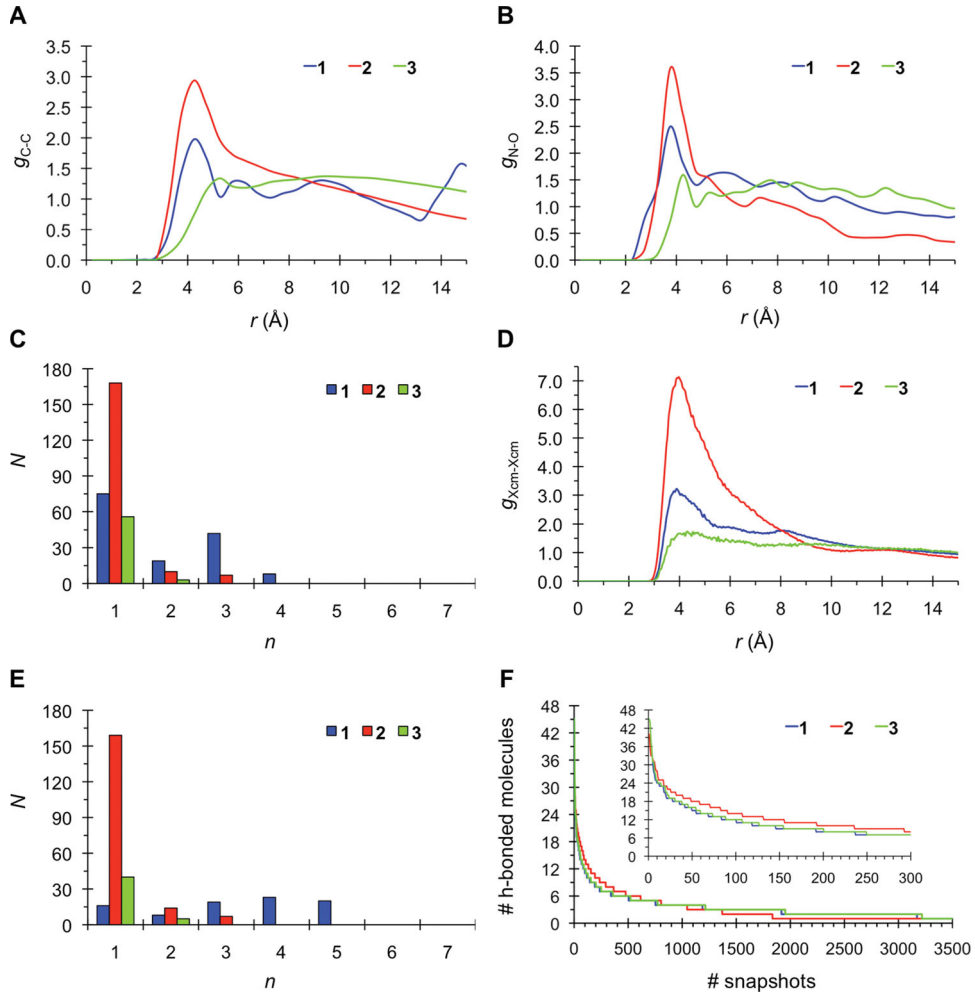

Figure 4. Radial distribution functions for the A) C···C and B) N···O pairs of atoms belonging to different ionene polymer chains. C) Number of N···O hydrogen bonds (*N*) with life times comprised between 0 and 0.5 ns ($n = 1$), 0.5 and 1.0 ns ($n = 2$), 1.0 and 1.5 ns ($n = 3$) and 1.5 and 2.0 ns ($n = 4$). D) Radial distribution functions for pairs of centers of masses of aromatic rings belonging to different ionene polymer chains. E) Number of π–π stacking interactions (*N*) with life times comprised between 0 and 0.5 ns ($n = 1$), 0.5 and 1.0 ns ($n = 2$), 1.0 and 1.5 ns ($n = 3$), 1.5 and 2.0 ns ($n = 4$) and 2.0 and 2.5 ns ($n = 5$). F) Number of water molecules involved in hydrogen bonding interactions with the amide groups of the polymer chains against the number of snapshots (a decreasing order is displayed for the three evaluated systems).

π–π stacking interactions. Intermolecular hydrogen bonds in **1**–**3** have been examined through the radial distribution functions for N···O pairs belonging to different chains, $g_{N\text{-}O}(r)$, which are represented in Figure 4b. The peak centered at 3.7 Å, which reflects the formation of intermolecular N–H···O hydrogen bonds, is higher for **2** than for **1**, whereas the peak found for **3** is shifted to 4.2 Å and significantly smaller than for the other two systems. Quantitative analysis of the number of intermolecular hydrogen bonds with a N···O distance ≤ 4 Å indicates that this kind of interactions are 1.3 and 3.3 times more abundant for **2** than for **1** and **3**, respectively. In order to compare the stability of these interactions, the life time (i.e., amount of time in which a given interaction remains formed without any disruption) of each detected interaction has been evaluated. After this, hydrogen bonds have been categorized in *n* groups, which reflect the number of interactions (*N*) with a life time comprised between $(n\text{-}1)\cdot 500$ ps and $n\cdot 500$ ps. Thus, hydrogen bonds belonging to groups with $n = 1$, 2, 3, or 4 refer to interactions with life times comprised within the following intervals: [0–0.5 ns], [0.5–1.0 ns], [1–1.5 ns] or [1.5–2.0 ns], respectively. Figure 4c, which depicts *N* against *n* for the three simulated systems, indicate that 46%/35%/6% of hydrogen bonds found in **1** show life times higher than 0.5 ns/1.0 ns/1.5 ns. In contrast, 91% of hydrogen bonds detected in **2** display life times lower than 0.5 ns while only 4% of such interactions remain for a time comprised between 1.0 and 1.5 ns. Finally, hydrogen bonds in **3** are not only scarce but also relatively unstable (i.e., only 5% exceed 0.5 ns and none reached 1.0 ns). According to these results, *N,N′*-(*-para-*phenylene)dibenzamide linkages affect not only to the abundance of intermolecular hydrogen bonds but also to the stability of such interactions.

On the other hand, the radial distribution functions calculated for pairs of centers of masses of aromatic rings belonging to different chains, $g_{Xcm\text{-}Xcm}$ (i.e., X_{cm} refers to the center of masses of aromatic rings), has been used to explore the possible existence of intermolecular π–π stacking interactions. As

it can be seen in Figure 4d, $g_{Xcm\text{-}Xcm}$ shows a high and relatively sharp peak centered at 3.9 Å for **2**, which becomes smaller for **1**. The practically flat profile obtained for **3** suggests that this kind of interactions is very scarce for polymers with *N,N′*-(*para*-phenylene)dibenzamide linkages. According to these results, the number of intermolecular π–π stacking interactions grows in the following order: **3** < **1** < **2**. Considering a threshold distance r < 6 Å, the number of interactions detected for **2** is 2.1 and 4.4 times higher than that found for **1** and **3**, respectively. Analysis of the angles (θ) formed by the planes of two interacting rings led to an average value of 47 ± 33°, 26 ± 14°, and 67 ± 26° for **1**, **2**, and **3**, respectively, evidencing important differences in the relative orientation of the two aromatic entities. More specifically, π–π stacking interactions in **2** are essentially dominated by a parallel disposition of the aromatic rings (i.e., relatively close to the ideal planar configuration with $\theta \approx 0°$) while rings prefer a perpendicular arrangement in **3** (i.e., relatively close to the ideal T-shaped configuration with $\theta \approx 90°$). Interestingly, the average angle displayed by **1**, as well as its large deviation, reflects an intermediate situation, suggesting the coexistence of parallel and perpendicular configurations. Categorization of the π–π stacking interactions according to the life time is provided in Figure 4e. As it can be seen, the life time of 88% of the interactions found in **2** is lower than 0.5 ns while 72% / 50% / 23% of the π–π stacking interactions detected in **1** show life times larger than 1.0 ns/1.5 ns/2.0 ns. Overall these results clearly indicate that the topological constraints derived from the substitution of the phenyl ring affects very significantly to the intermolecular interactions pattern (i.e., abundance and stability of both hydrogen bonds and π–π stackings), which is also expected to have a large influence on the gelation phenomenon. The average life times calculated for intermolecular hydrogen bond / π–π stacking interactions of **1**, **2**, and **3** are 0.7/1.7, 0.1/0.3 and 0.2/0.2 ns, respectively. These averages combined with results displayed in Figure 4 allow us to conclude that the stability of the assemblies predicted by MD simulations decreases as follows: **1** >**2** >>**3**.

On the other hand, the formation of specific hydrogen bonding interactions between the polymer chains and the explicit solvent molecules has been analyzed snapshot-by-snapshot. Figure 4e represents the number of water molecules hydrogen bonded to the amide groups contained in the polymer chains of each system against the number of analyzed snapshots. As it can be seen, the maximum of hydrogen-bonded waters is 45, 40, and 45 for **1**, **2**, and **3**, respectively, even though such high number is only observed in one snapshot. Moreover, only 145, 235, and 154 snapshots are able to retain 10 or more water hydrogen bonded to the amide groups of **1**, **2**, and **3**, respectively. These results indicate that the hydration of polymer chains, which is illustrated in Figure 3, essentially occur through non-specific water···polymer interactions. Moreover, the inset displayed in Figure 4e clearly shows that the formation of water···amide interactions is slightly more favored for **2** than for **1** and **3**.

The temporal evolution of the radius of gyration (R_g) has provided qualitative information of the molecular flexibility of **1**–**3** (Figure S14, Supporting Information). The resulting average R_g value ± 2·standard deviation is 21.1 ± 3.56 Å, 27.8 ± 4.36, and 35.8 ± 2.81 Å for **1**, **2**, and **3**, indicating that the flexibility grows in the following order: **3** < **1** < **2**. Evaluation of the hydrodynamic radius (R_H) leads to similar conclusions, the average value being 21.5 ± 1.5 Å, 24.6 ± 2.0, and 28.8 ± 1.2 Å for **1**, **2**, and **3**, respectively. Correlation of these structural parameters with the intermolecular interactions discussed above allows us to predict that the ability to form polymer assemblies increases with the molecular flexibility, which in turn is directly related with the structural isomerism of the phenylenediamine core. However, the stability of the formed polymer assemblies is also significantly affected by the molecular flexibility, as is clearly evidenced by the analyses of the residence times. More specifically, although **1** shows less intermolecular interactions than **2**, the molecular flexibility of the latter perturbs their strength and stability, which are weaker than those of **1**. Accordingly, the hydrogelation capacity is controlled by the density of intermolecular interactions, which allows to discriminate **3** with respect to **2** and **1**, and also by the stability of such interactions, which is significantly higher for **1** than for **2**.

In order to examine the reliability of the studied models, additional simulations were carried out using an extended system of **2** (model **2e**), which was selected because of its abundant intermolecular interactions. Results obtained for model **2e** (Figure S16 and S17, Supporting Information), which consists of four polymer chains with n = 6 immersed in a simulation box with 98498 explicit water molecules (Figure S15, Supporting Information), are fully consistent with those reported in Figure 4 for **2** corroborating the assembling ability predicted for the system with *N,N′*-(*meta*-phenylene)dibenzamide linkages). Thus, enlargement of the number of polymer chains does not alter the structural organization and the main characteristics of the interaction pattern obtained for **2**, which is based on the coexistence of regions dominated by a large number of polymer···polymer with hydrated polymer zones. The maximum number of water molecules forming hydrogen bonds with the polymer chains is 10 and 15 per molecule of **2** and **2e**, respectively. However, the average R_g and R_H values calculated **2e** (32.6 ± 3.6 and 31.4 ± 1.5 Å, respectively) indicate that, as expected, the length of the molecular chain increases slightly with the number of assembled molecules while the flexibility decreases.

On the other hand, the influence of the molecular weight in the hydrogelation ability of ionenes **1** and **2** has been evaluated by considering models made of two polymer chains with n = 8 (**1w** and **2w**, respectively) immersed in a simulation box filled with explicit water molecules, respectively. Results obtained for **1w** and **2w** (Figure S18, Supporting Information) are similar to those displayed in Figure 4, this feature being particularly outstanding for the latter system. Accordingly, the assembly behavior discussed above for the polymer with *N,N′*-(*meta*-phenylene)dibenzamide and *N,N′*-(*ortho*-phenylene)dibenzamide linkages are practically independent of the number of repeat units in terms of abundance and stability of the intermolecular polymer···polymer interactions.

Density Functional Theory (DFT) calculations using small model dimmers, which are described in the ESI, were carried in both the gas-phase and aqueous solutions to get additional information on the relative hydrophobicity and hydrogelation ability of the three investigated systems. Evaluation of the free energies of solvation (ΔG_{sol}) indicated that the interaction of

such dimmers with the solvent is more favorable for **3** than for **2** and **1** by 0.8 and 3.6 kcal mol^{-1}, respectively. Accordingly, the relative hydrophobicity of these dimmers, which decreases with increasing separation the aromatic rings containing in the repeat unit, follows the same order that the gelation ability: **1** >**2** >**3**. This feature together with the calculated binding energies and intermolecular geometries (Table S1 and Figure S20, Supporting Information) indicate that the hydrogelation ability of **1** and **2** are higher than that of **3**. Moreover, the complex and dense network of hydrogen bonding and π–π stacking interactions found for **1** (Figure S20, Supporting Information) suggest that *N,N′*-(*ortho*-phenylene)dibenzamide linkages are the most appropriated to form stable hydrogels.

2.3. Experimental Hydrogelation

Ionenes **1**–**3** were subjected to thermal hydrogelation tests that consisted in cooling to RT the isotropic solutions of a weighted amount of a given ionene in 1 mL of doubled-distilled water (organogelation tests were negative). The material phase was first classified as a gel if no gravitational flow was observed upon turning the vial upside-down, and further confirmed by rheological measurements. **1** induced the most effective gelation at the lowest critical gelation concentration (CGC = 25 ± 2 g L^{-1}), which corresponded to a ≈ fourfold and twofold drop with respect to **2** and **3**, respectively (**Figure 5**). All hydrogels were thermoreversible over several heating-cooling cycles without any noticeable detriment of their properties. A typical hysteresis loop between gel-to-sol and sol-to-gel transition temperatures of 10–15 °C was also observed under controlled heating-cooling rates. Remarkably, and in agreement with the rheological data (vide infra), we observed that the gel-to-sol transition of the hydrogel made of **1** could be also induced by sonication instead of heating as external stimulus, and the gel phase restored upon quiescence. In sharp contrast, sonication

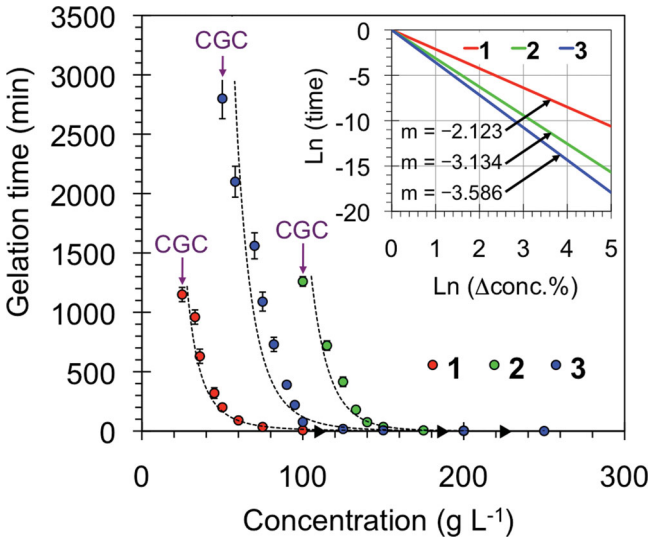

Figure 5. Gelation kinetics for each ionene gelator. Inset: Normalized Ln–Ln plot of the gelation time against the corresponding percentage increases in concentration.

treatment of the hydrogels made of **2** or **3** lead to a heterogeneous mixture of solvent, precipitate and pieces of jelly-like material that did not returned to a uniform hydrogel over time.

Simple changes in the molecular geometry of the ionenes not only influenced the CGC, but also the gelation kinetics. Figure 5 suggests complex decay kinetics of the supramolecular assembly with increasing concentration of a given ionene. Ln–Ln plots revealed that for an equivalent increment in concentration with respect to the CGC the materials based on **3** and **2** evolved ≈ 1.7-fold and 1.5-fold faster, respectively, than **1** to reach gelation within ≈ 2–3 min (Figure 5). However, in absolute terms, the much lower CGC of **1** makes this ionene the best choice to achieve rapid gelation within a wide range of concentrations. For instance, the gelation times achieved at 100 g L^{-1} were ca. 5 min, 1.3 h and 21 h for **1**, **3**, and **2**, respectively. Even at the CGC, **1** showed the faster gelation (e.g., ≈ 19 h for **1** vs 47 h for **3**).

2.3.1. Physical Properties of Hydrogels

Anticipating unique structure-property relationships, the hydrogels made of each ionene were subsequently characterized in terms of their thermal-mechanical stability, optical and morphological properties.

The thermal stability of the hydrogels prepared from the isomeric ionenes at a concentration of 100 g L^{-1} (this corresponds to the CGC of **2**, which is the largest CGC value among the three ionenes) was comparable between **2** and **3**, and slightly superior in ≈ 5–6 °C for **1**. However, a more realistic vision could be obtained by looking at the percentage increases of the variable over the entire range of permitted concentration until reaching a plateau value of T_{gel}. As expected for physical gels, the gel-to-sol transition temperature (T_{gel}) values increased considerably with the gelator concentration. Very interestingly, homogeneous and stable hydrogels could be formed at very high concentrations, defined by the solubility limit of the ionene in hot water, following the order **1** (1500 g L^{-1}) >**2** (750 g L^{-1}) >**3** (400 g L^{-1}) (**Figure 6**A). This feature allowed for the preparation of hydrogels with a wide range of T_{gel} values (ΔT_{gel} = 58–74 °C) even well above the boiling point of water. The Ln–Ln plot of the percentage increases before the plateau regions showed an almost perfect linear relationship between the increment in the gelator concentration and the consequent increment in the T_{gel} with respect to the initial values at the CGC (Inset Figure 6A). Thus, within the end-limits defined by the CGCs and the maximum T_{gel} values, the slopes of these straight lines indicated that **3** causes a 1.2-fold and 1.6-fold higher percentage increment of T_{gel} than **2** and **1**, respectively.

Oscillatory rheological measurements confirmed the viscoelastic gel state of the materials. Their storage modulus (G') and loss modulus (G'') were first measured at RT as a function of the frequency (dynamic frequency sweep experiment, DFS) and shear strain (dynamic strain sweep experiment, DSS) to determine the linear viscoelastic regime (solid-like response) associated to each material (**Figure 7**A and 7B). Reproducible and relatively constant dissipation factors (tan $\delta = G''/G' \approx 0.1$) during the dynamic frequency sweep indicate a good tolerance

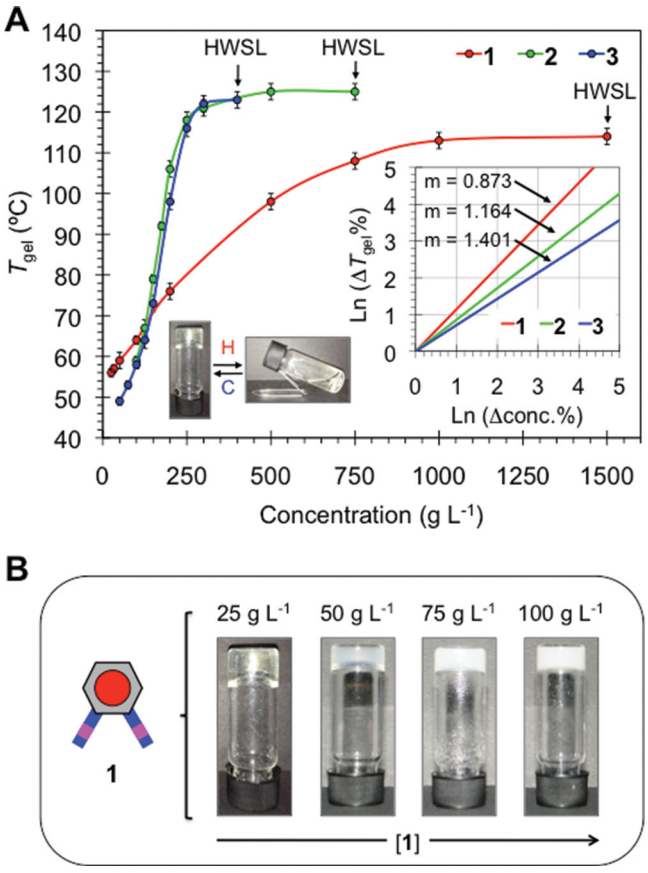

Figure 6. A) Evolution of T_{gel} with ionene concentration. Inset plot: Normalized Ln–Ln graphic of the corresponding percentage increases. Inset photographs: Representative phase thermoreversible transition for the hydrogel prepared from **1** at 25 g L^{-1}. Abbreviation: HWSL = hot-water solubility limit; *m* = slope; *H* = heating; *C* = cooling. B) Increment of opacity with the ionene concentration for the hydrogel prepared from **1**.

of the hydrogels to external forces. Within the linearity limits of deformation, G' was always about one order of magnitude higher than G'' over the entire range of frequencies. Further dynamic time sweep (DTS) measurements at critical strain at yield ($\gamma = 0.1\%$) and 1 Hz frequency confirmed the stability of the hydrogels as a function of the ageing time at RT. In general, for the same ionene G' increased and tan δ decreased with increased concentration, whereas the crossover point of G' and G'' shifted to lower strain, indicating an enhancement of the mechanical damping properties and brittle nature of the materials (Figure S9, Supporting Information). It is worth mentioning that both thermal and flow properties of hydrogels based on oligomeric electrolytes are also influenced by the salt content.[31] Focusing on the effect of the polymer topology, the mechanical strength of the hydrogels prepared from ionenes **1**–**3** at 100 g L^{-1} (higher CGC among the studied ionenes) decreased in the order **1** ($G' \approx 14$ kPa) >**3** ($G' \approx 11$ kPa) >**2** ($G' \approx 2.5$ kPa). However, when the hydrogels were prepared at their respective CGC the tan δ increased in the order **2** < **1** < **3**, which indicates that concentration affects differently to the gel properties depending on the topology of the ionene polymer (Figure S10, Supporting Information).

Remarkably, we also found that only the hydrogel made of **1** displayed a thixotropic response against the mechanical stress caused by large-amplitude oscillations. Figure 7C shows a loop test based on successive cycles of low-high strain separated by enough time to ensure complete gel-to-sol ($G' < G''$) and sol-to-gel ($G' > G''$) transitions while minimizing inertial effects between the steps. The results showed that the original gel properties were fully recovered within 220 ± 3 min after termination of the large stress. The enthalpy change for the exothermic gel-recovery was found to be $\Delta E_H = -13.0 \pm 0.5$ kJ mol^{-1} from the Arrhenius equation (Figure 7D). Such self-healing behavior at RT was also macroscopically observed within ca. 16 h after a vigorous shaking-resting process applied directly to the glass vial containing the hydrogel. These results suggest that ionene **1** behaves similarly to other ionene gelators (i.e., poly[pyridinium-1,4-diyliminocarbonyl-1,4-phenylene-methylene chloride),[32] albeit the underlying relationship between ionene structure and thixotropic behavior still remains unclear pending further investigation.

In terms of optical appearance, the difference in the CGC values associated to each ionene was accompanied by the formation of transparent gels from **1**, whereas opaque white gels were obtained in the case of **2** and **3** at their respective CGC (Table S1 and Figure S8, Supporting Information). As expected, an increase in the concentration of **1** increased also the opacity of the hydrogel (Figure 6B), suggesting the gradual formation of aggregates greater than the wavelength of visible light (≈ 380–780 nm). Moreover, the hydrogels showed distinctive birefringence domains under crossed nicols depending on the ionene structure and concentration (**Figure 8** and Figure S13, Supporting Information), indicating the presence of different anisotropic aggregates. The reduced birefringence observed for the hydrogels made of **2** in comparison to **1** and **3** at the same concentration suggested the formation of less extended networks in the former, which was in agreement with their weaker mechanical strength (vide supra). Noteworthy is that the possibility of tuning the optical properties of these thermo-sensitive hydrogels based on the topology of the ionene gelator may help to expand also their range of potential applications to optoelectronic devices.[33]

Further electron microscopy imaging of the xerogels, obtained by freeze-drying the corresponding hydrogels, confirmed the induction of different anisotropic morphologies caused by each ionene (Figure 8). TEM images clearly revealed overlapped laminar structures consisting on large and homogeneous sheets for the xerogels from **1** and **3**, whereas the xerogel from **2** showed a complete different morphology consisting on rough domains without discernible fibrilar or laminar regions. In good agreement, further FE-SEM images of the specimens confirmed the described morphology in greater detail. Thus, dense macroporous networks formed by connected leaf-like structures with interlaminar distances in the range of ≈5–10 μm were observed for the xerogels from **1** and **3**. In sharp contrast, globular shaped agglomerates resembling pebble stones ($\phi \approx 0.5$–1 μm for individual particles) were characteristic of the xerogel obtained from **2**. Augment of the cross-linking density and loss of anisotropy was observed in all cases upon extensive increase of ionene concentration, as evidenced by the formation of distorted microstructures of reduced birefringence.

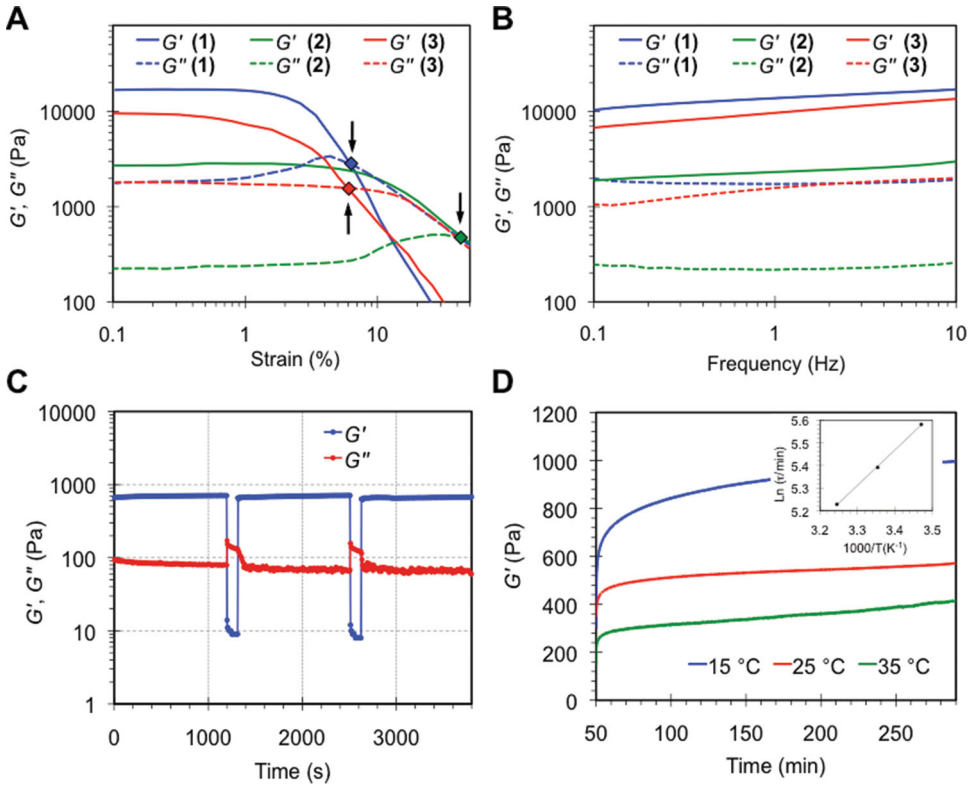

Figure 7. Rheological characterization of hydrogels made from **1**–**3** at the same concentration (c = 100 g L^{-1}). A) DSS test at 1 Hz frequency and RT. B) DFS tests at 0.1% strain and RT. C) Thixotropy-loop test of the hydrogel prepared from **1** at CGC. D) Evolution of the storage modulus at different temperatures after termination of the large stress (t = 30 min). Inset: Arrhenius plot of the relaxation time.

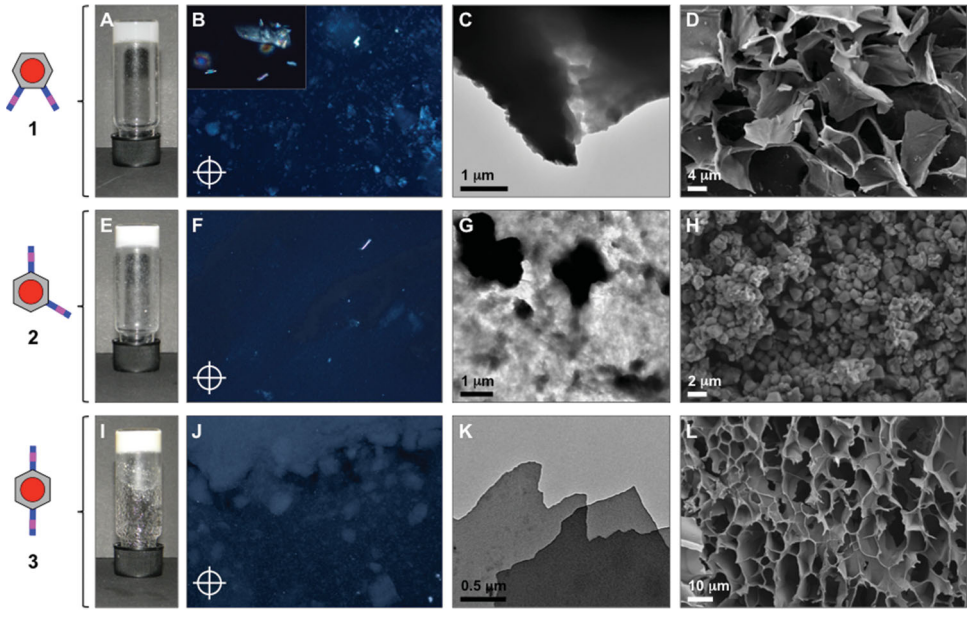

Figure 8. Optical and morphological features of hydrogels prepared from ionenes **1** (A–D), **2** (E–H) and **3** (I–J) at c = 100 g L^{-1}. A,E,I) Digital photographs of upside-down vials with the hydrogels. B,F,J) Optical images (10×) of the hydrogel films under crossed nicols. Inset in (B): Optical image (50×) of the hydrogel prepared from **1** at CGC (c = 25 g L^{-1}). C,G,K) TEM and D,H,L) FE-SEM microphotographs of the corresponding xerogels.

2.3.2. Dispersion of Single-Walled Carbon Nanotubes (SWNTs)

The insolubility of SWNTs in aqueous solutions due to entanglement and hydrophobic association of the nanotubes is considered one of the major practical limitations of these promising materials, especially in fields such as biomedical engineering and biochemistry.[34,35] Hence, a considerable research effort has been devoted during the last decade to the development of cost-effective methods to readily disperse SWNTs either by covalent or non-covalent strategies that preserve their functional properties.[36] Within non-covalent approaches different research groups have explored the use of surfactants[37] and polycations[38–40] as dispersants. Moreover, the preparation of SWNTs-hydrogel composites has also received a growing interest due to the potential synergic combination of properties from both materials.[36,41–43]

In comparison to ionenes **1**–**3**, other polyelectrolyte dispersants are built either from a different rigid core or different spacers. During our research, we were delighted to confirm that the modification of the substitution angle in the phenylenediamine core of DABCO-containing ionene gelators resulted also crucial to provide such additional functionality to these specific hydrogels (i.e., use of DABCO as molecular spacer). Despite the structural similarities with other polyelectrolyte dispersants, in which the planar π–surface of the phenylene core seems to be crucial for the π–stacking interaction with the carbon nanotubes,[26] opaque hydrogels based on ionenes **2** and **3** at their CGC were unable to hold a dispersion of SWNTs. However, the use of the ionene gelator **1** at CGC allowed for the facile preparation of thermoreversible and homogeneous SWNTs-hydrogel composites (**Figure 9**A). Interestingly, other transparent hydrogels obtained using flexible diamine spacers (e.g., *N,N,N′,N′*-tetramethyl-1,6-hexanediamine, *N,N,N′,N′*-tetramethyl-1,3-propanediamine) and PPDA showed a similar dispersion ability. In general, an increase of the gelator concentration leading to more opaque gels was accompanied by a gradual detriment of the dispersibility. Thus, the aggregates size and morphology seem to play a key role among the parameters influencing the dispersion of SWNTs within surfactant-free ionene hydrogels.

In contrast to previous systems,[26] hybrid hydrogels could be prepared by addition of the SWNTs on top of the hydrogel made of **1** followed by sonication and a final quiescent state at RT (Figure 9E). The so-prepared materials maintained the same T_{gel} either upon heating-cooling or sonication-resting cycles. Interestingly, we observed that the use of the preformed hydrogel was crucial in order to disperse by sonication the over layered SWNTs and form the stable hybrid gel. Thus, the addition of the SWNTs to an isotropic solution of **1** at the CGC (prepared by heating or sonication) resulted in the hydrogel formation with precipitated instead of dispersed SWNTs (Figure 9E, top). The use of concentrations higher than CGC accelerated in all cases the gelation process but, as mentioned above, it did not improve the dispersion of the nanotubes. Thus, the hydrogel prepared from **1** at CGC behaves as a unique system for the dispersion of SWNTs and subsequent formation of SWNTs-hydrogel composites.

It is worth to mention that although sonication usually leads to transient exfoliation of the nanotubes, the favorable interaction with the ionene gelator, like with other polymeric dispersants, may stabilize the exfoliated tubes preventing further aggregation.[44] Moreover, sonication-induced sol-to-gel transition could be repeated several times, without the necessity of the heating-cooling process, which indicated the preservation of the thixotropic gel network. The maximum concentration of SWNTs that could be homogenously dispersed was 0.1 g L^{-1}, which did not cause a major change on the thermal-mechanical stability of the gel matrix (i.e., $\Delta T_{gel} \approx 2$–5 °C; $\Delta\tan\delta \approx 0.04$) (Figure S11 and S12, Supporting Information). Under these conditions, the gel-like SWNTs dispersions showed vis–NIR absorption (Figure S13, Supporting Information), maintained the uniform black color for several months (e.g., no precipitation of nanotubes was observed after 3 months) and displayed birefringence under polarized light (Figure 9B). Precipitation of the SWNTs and a clear supernatant solution were obtained when the dispersion was attempted by sonication or heating in

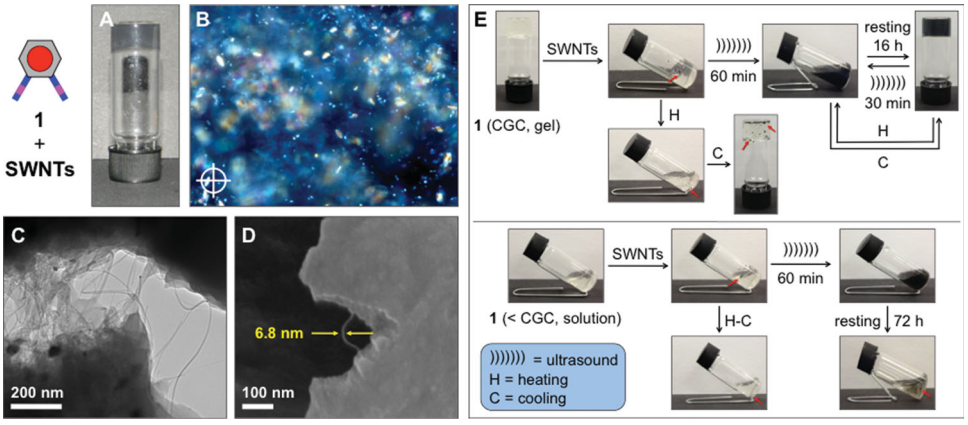

Figure 9. Optical and morphological characterization of SWNTs-hydrogel composite made of **1** (c = 25 g L^{-1}) and SWNTs (c = 0.1 g L^{-1}). A) Upside-down vial containing the hybrid hydrogel. B) Optical image (20×) of the composite film under crossed nicols. C) TEM and D) FE-SEM images of the hybrid xerogel. E) Top: General preparation of SWNTs-hydrogel composite and its reversibility. Bottom: Dispersion of the SWNTs was not possible by sonication or heating-cooling treatment of the mixtures at concentrations of **1** below CGC.

the presence of **1** below the CGC (e.g., $c = 10$ g L^{-1}) (Figure 9E, bottom). Therefore, the gel network (and not only the polyelectrolyte) provides the necessary microenvironment for the optimal stabilization of the nanotubes dispersion. Moreover, electron microscopy imaging (i.e., TEM, FE-SEM) of the specimens clearly visualized the perfect embedment of the SWNTs within the highly dense gel matrix (Figure 9C,D). The above results were in concordance with both the conserved anisotropy of the gel phase and the high stability of these dispersions without aggregation of the nanotubes.[45]

2.4. Mechanistic Considerations

It has been already anticipated that cooperative hydrogen bonding, π–π, cation–π, and other electrostatic interactions may play an important role in the gelation mechanism of ionenes.[26] In fact, the bonding energy for only H-bonding (≈20 kJ mol^{-1}) is much higher than the global activation energy for the gel formation estimated by rheology. As expected, comparative FT-IR spectra confirmed the expected participation of hydrogen-bonded amides and aromatic interactions during the gelation process. Thus, hydrogen bonding in the ionene hydrogels shifted both CO and NH resonances to lower energy with respect to the solid ionene (e.g., from ≈ 1656 to 1531 cm^{-1} for amide I bands, and from ca. 3390 to 3275 cm^{-1} for NH stretching bands). Although the gel-to-sol transition occurred with increasing temperature, the IR bands arising from hydrogen-bonded amide groups decreased only slightly in the isotropic solution indicating that these interactions are already significant in the solution phase (ESI). In agreement with previous observations,[46] additional contributions arising from dynamic interactions between amide groups and water molecules through the chloride anions is also reasonable based on the observation of amide proton signals at ca. 12.3 ppm in the NMR spectrum in DMSO-d_6 (ESI). Moreover, anion/cation–π interactions in these ionenes should also be considered, especially in a polar medium where most other intermolecular forces are considerably attenuated. In this sense, it is important to realize that strongly associated ion pairs can diminish the strength of the cation–π bonding by up to 80%.[47] In our case, this interaction could be rather important in the gelation mechanism because the ionenes were unable to form hydrogels upon exchange of chloride by TFSA anions, which should hinder the ammonium-π interactions due to the expected stronger association of the TFSA-tetraalkylammonium ionic pair in comparison to chloride-tetraalkylammonium in water.

In order to get more conclusive information about the gelation mechanism, MD results for the three simulated ionene polymers have been used to examine the possible existence of interactions different to those discussed above (i.e., intermolecular hydrogen bonds and intermolecular π–π stacking in Figure 4b,c, respectively). **Figure 10**a,b represent the radial distribution functions for $N^+\cdots X_{cm}$ ($g_{N+/X}$) and $Cl^-\cdots X_{cm}$ ($g_{Cl-/X}$) pairs, respectively, where X_{cm} refers to the center of masses of aromatic rings. It is worth noting that $g_{N+/X}(r)$ and $g_{Cl-/X}(r)$ are related with the formation of cation–π and anion–π interactions, respectively. The number of pairs with a $N^+\cdots X_{cm}$ distance lower than 5.0 Å is very low for **1** and **2**, the only system with

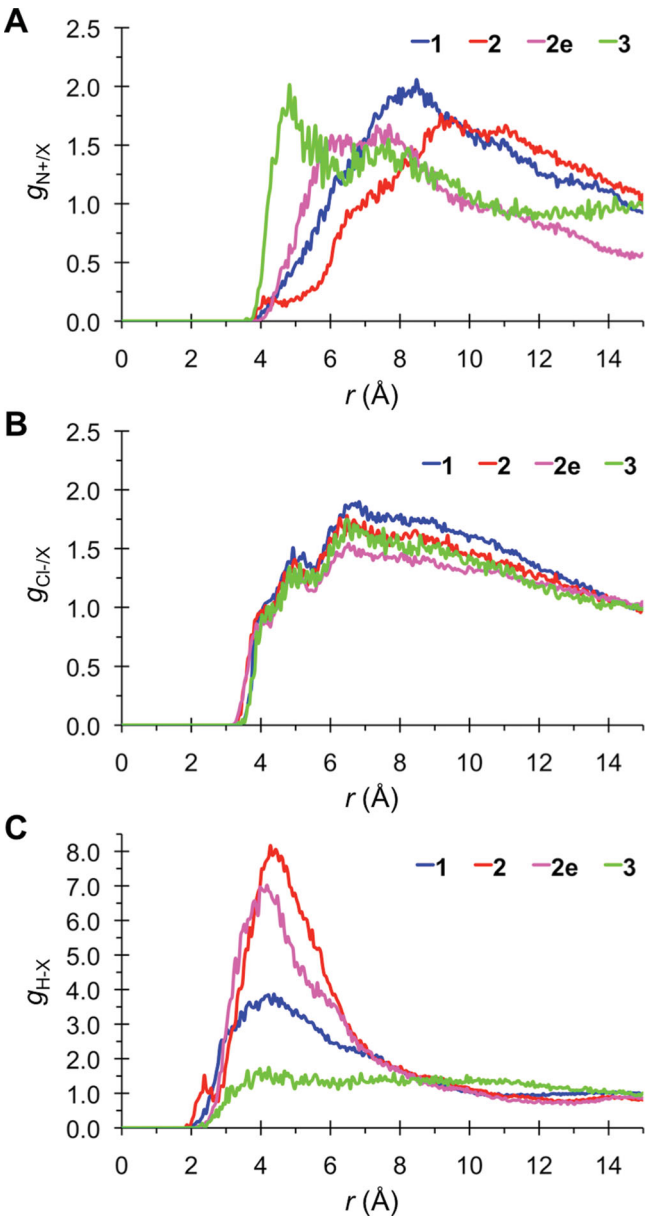

Figure 10. Radial distribution functions for the A) $N\cdots X_{cm}$, B) $Cl^-\cdots X_{cm}$ and C) (N–)H $\cdots X_{cm}$ pairs, belonging to different ionene polymer chains, where X_{cm} refers to the center of masses of aromatic rings.

a peak below such threshold distance being **3**. Indeed, cation–π interactions are 5.2 and 7.5 times more abundant for **3** than for **1** and **2**, respectively. Combination of this result with the experimental evidences discussed above suggests that the importance of cation–π interactions in the gelation process is relatively low. In order to corroborate this feature, the $g_{N+/X}(r)$ profile was calculated for **2e**, results being included in Figure 10a. Comparison of the profiles obtained for **2** and **2e** indicates that number and strength of cation–π interactions decreases and increases, respectively, with the number of polymer chains contained in the model. Despite of this, the strength of such kind of interactions is significantly lower for **2e** than for **3**, confirming their little influence in the gel formation.

The $g_{Cl\text{-}/X}(r)$ profiles calculated for **1**–**3** (Figure 10b) are relatively similar, evidencing the existence of $Cl^- \cdots X_{cm}$ pairs at distances as short as 3.22 Å. From a quantitative point of view, the population of $Cl^- \cdots X_{cm}$ pairs at distances shorter than 5.0 Å is similar for **1** and **2** (i.e., 4% larger for the latter) but 15% lower for **3** than for **2**. Furthermore, the amount of anion–π interactions in **2** is 1.1 times higher than the number of cation–π interactions in **3**. Comparison of the profiles obtained for **2** and **2e** indicates that both the strength and the amount of Cl^-–π interactions do not change when the number of polymer molecules in the simulated model increases from two to four. Although the amounts of anion-π interaction detected for the three molecular systems show differences that are smaller than for intermolecular hydrogen bonds and π-π stacking, they grow as displayed in Figure 4 for the latter interactions (i.e., **2** >**1** >**3**), Accordingly, anion–π interactions may play a crucial role in the gelation mechanism since their strength is not negligible as compared to intermolecular hydrogen bonding and π–π stacking interactions.[48,49] The average residence time for anion–π interactions is 431, 173, and 316 ps for **1**, **2**, and **3**, respectively.

Attractive interactions between the N–H of amide groups and the π-cloud of aromatic rings belonging to different chains have been also invoked to explain the gelation mechanisms. The possible existence of such kind of intermolecular interactions in **1**–**3** has been analyzed by examining the radial distribution functions for (N–)H $\cdots X_{cm}$ pairs, $g_{H\text{-}X}(r)$, which are displayed in Figure 10c. As it can be seen, no peak is detected for **3** evidencing that the formation of such kind of interactions is not particularly favored in the polymer *N,N′*-(*para*-phenylene)dibenzamide linkages. In contrast, **1** and **2** show a well-defined peak centered at 4.17 and 4.32 Å, respectively. The height of the peak is significantly more pronounced for **2** than for **1** evidencing that N–H$\cdots\pi$ interactions are considerably more abundant in the former than in the latter. More specifically, integration of the area of the peaks within the distance interval defined by the crossing of the two profiles at $r = 7.47$ Å indicates that the population of N–H$\cdots\pi$ interactions through the trajectories is 60% higher for **2** than for **1**, even though the average residence time is slightly higher for the latter than for the former (i.e., 368 and 319 ps for **1** and **2**, respectively). Inspection of the $g_{H\text{-}X}(r)$ profile calculated for **2e** (Figure 10c) indicates that the preference of the ionene polymer with *N,N′*-(*meta*-phenylene)dibenzamide linkages is practically independent of the number of explicit molecules used in the simulated model. Thus, a pronounced peak centered at 4.17 Å, similar in high to that found for **2**, is also detected for **2e**.

On the other hand, detailed analyses of the stored snapshots evidenced that the amount of weak specific interactions at the intramolecular level (i.e., hydrogen bond, π–π stacking and N–H$\cdots\pi$) is very small or practically null. This feature reflects that the role of intramolecular interactions in the gelation of the three ionenes studied in this work is null. This result combined with both the experimental observations previously discussed and the radial distribution functions represented in Figure 4, 10 indicate that the hydrogels studied in this work results from the combination of multiple specific intermolecular interactions. Specifically, hydrogen bonding, π–π stacking, anion–π and N–H$\cdots\pi$ interactions play a fundamental role in the formation of **1**–**3** hydrogels. Furthermore, the stability of the formed assemblies is also crucial for understanding the gelation ability. Accordingly, interactions are clearly more numerous in **2** than in **1** while, in opposition, they are more stable in **1** than in **2**, **3** being the less favored in all cases. These results clearly reflect the large influence of the substituted phenylenediamine isomerism in the strength, abundance and stability of intermolecular interactions, being responsible of the differences observed in the gelation of such ionene systems. It is worth mentioning that we have also observed a superior ability of **1** to gel not only water but also HCl solutions, which constitute the subject of a separate investigation.

3. Conclusion

In conclusion, a combined computational-experimental approach can be applied to optimize the structure of ionene polymers in order to enhance their gelation efficiency and achieve hydrogels with superior properties without adding external additives. As a proof of concept, surfactant-free ionene polymers **1**–**3** containing DABCO and *N,N′*-(*x*-phenylene) dibenzamide linkages (*x* = *ortho*-/*meta*-/*para*-) were used as model systems. Molecular dynamics simulations of the isomeric ionenes with explicit water molecules allowed for the comparison of polymer$\cdots$water and polymer$\cdots$polymer interactions (e.g., hydrogen bonding, π–π stacking, cation–π, anion–π) in each case through the corresponding radial distribution functions. The results showed that the topological constraints derived from the substitution pattern of the core aromatic ring drastically affects the intermolecular interactions pattern, which is also expected to have a large influence on the gelation phenomenon. Specifically, although domains with high degree of hydration were visualized for the three systems, polymer$\cdots$polymer interactions were only evident in the case of *ortho*- (**1**) and *meta*- (**2**) isomeric ionenes. The predictive models were consistent upon a range of repeating units and explicit polymer chains. In good agreement with the theoretical assembly models, **1** provided experimentally the best hydrogels among the three ionenes **1**–**3**. Heating-cooling treatment allowed for the preparation of thermoreversible hydrogels in each case, but only in the case of **1** sonication was also found to induce gelation very efficiently. Moreover, **1** displayed the lowest critical gelation concentration (CGC = 25 ± 2 g L^{-1}), the highest thermal stability at CGC, superior optical properties, a rapid gelation kinetics within a wide range of concentration, a self-healing behavior, and the ability to disperse pristine SWNTs. Neither optical transparence, nor self-healing, nor dispersibility of SWNTs could be achieved with *meta*- (**2**) and *para*- (**3**) DABCO-containing ionenes. In principle, this approach could be applied for the topological optimization of other gelators based on either polymers or low-molecular-weight compounds in order to tune the molecular self-assembly and achieve multifunctional gels with superior properties. Detailed investigations on additional properties of gelator **1**, property-ionization state relationship studies, and the preparation of biohybrid materials are currently underway in our laboratories.

Supporting Information

Supporting Information is available from the Wiley Online Library or from the author.

Acknowledgements

Financial support from Universität Regensburg (Anschubfinanzierung von Wissenschaftlichen Projekten-2011), Ministerio de Ciencia e Innovación – FEDER (projects CTQ2010–17436 and MAT2012–34498), Gobierno de Aragón – FSE (research group E40), and the DIUE of the Generalitat de Catalunya (contracts 2009SGR 925 and XRQTC) is gratefully acknowledged. Computational support is thanked to CESCA. We are also indebted to S.A. Bäurle and E. Peter (Universität Regensburg) for preliminary calculations; A. Göpferich (Universität Regensburg) for granting us access to the AR 2000 rheometer; Judith Mayr (Universität Regensburg) for confirming some results; and M. Kar (NCL, India) for assistance with some measurements. Support for the research of C.A. was received through the prize "ICREA Academia" for excellence in research funded by the Generalitat de Catalunya. D.D.D. thanks DFG for the Heisenberg Professorship Award.

Received: December 19, 2013
Revised: March 19, 2014
Published online: April 28, 2014

[1] R. R. Netz, D. Andelman, *Phys. Rep.* **2003**, *380*, 1–95.
[2] A. Y. Grosberg, T. T. Nguyen, B. I. Shklovskii, *Rev. Mod. Phys.* **2002**, *74*, 329–345.
[3] C. Poinsignon, *Mat. Sci. Eng., B* **1989**, *B3*, 31–37.
[4] W. Jaeger, J. Bohrisch, A. Laschewsky, *Prog. Polym. Sci.* **2010**, *35*, 511–577.
[5] C. Werner, *Advances in Polymer Science: Polymers for Regenerative Medicine*, Springer, Dresden **2006**.
[6] S. Punyani, H. Singh, *J. Appl. Polym. Sci.* **2006**, *102*, 1038–1044.
[7] H. Kourai, T. Yabuhara, A. Shirai, T. Maeda, H. Nagamune, *Eur. J. Med. Chem.* **2006**, *41*, 437–444.
[8] A. N. Zelinkin, D. Putnam, P. Shastri, R. Langer, V. A. Izumrudov, *Bioconjugate Chem.* **2002**, *13*, 548–553.
[9] E. Bortel, A. Kochanowski, B. Siniarska, E. Witek, *Polish J. Appl. Chem.* **2001**, *44*, 55–77.
[10] H. Noguchi, *Ionene Polymers. In Polymeric materials encyclopedia*, (Ed: J. C. Salomone), CRC Press, Boca Raton, London, New York, Tokyo **1996**, pp 3392–3421.
[11] A. Laschewsky, *Curr. Opin. Colloid Interface Sci.* **2012**, *17*, 56–63.
[12] S. R. Williams, T. E. Long, *Prog. Polym. Sci.* **2009**, *34*, 762–782.
[13] E. R. Littmann, C. S. Marvel, *J. Am. Chem. Soc.* **1930**, *52*, 287–294.
[14] C. F. Gibss, E. R. Littmann, C. S. Marvel, *J. Am. Chem. Soc.* **1933**, *55*, 753–757.
[15] M. Friedman, *J. Agric. Food Chem.* **2003**, *51*, 4504–4526.
[16] J. K. Oha, R. Drumright, D. J. Siegwart, K. Matyjaszewski, *Prog. Polym. Sci.* **2008**, *33*, 448–477.
[17] M. Yoshida, *Synthesiology* **2012**, *5*, 181–189.
[18] S. Schlick, *Ionomers: characterization, theory, and applications* CRC Press, Boca Raton, FL **1996**.
[19] M. R. Tant, K. A. Mauritz, G. L. Wilkes, *Ionomers: Synthesis, structure, properties, and applications*, Blackie Academic and Professional, London **1997**.
[20] A. Kowalenko, A. E. Kobryn, S. Gusarov, O. Lyubimova, X. Liu, N. Blinov, M. Yoshida, *Soft Matter* **2012**, *8*, 1508–1520.
[21] Y. He, H.-K. Tsao, S. Jiang, *J. Phys. Chem. B* **2012**, *116*, 5766–5770.
[22] S. G. Lee, G. F. Brunello, S. S. Jang, D. G. Bucknall, *Biomaterials* **2009**, *30*, 6130–6141.
[23] S. S. Jang, W. A. Goddard, M. Y. S. Kalani, D. Myung, C. W. Frank, *J. Phys. Chem. B* **2007**, *111*, 14440–14440.
[24] S. S. Jang, W. A. Goddard, M. Y. S. Kalani, *J. Phys. Chem. B* **2007**, *111*, 1729–1737.
[25] E. Chiessi, F. Cavalieri, G. Paradossi, *J. Phys. Chem. B* **2007**, *111*, 2820–2827.
[26] Y. Misawa, N. Koumura, H. Matsumoto, N. Tamaoki, M. Yoshida, *Macromolecules* **2008**, *41*, 8841–8846, and references therein.
[27] T. Takewaki, L. W. Beck, M. E. Davis, *Microporous Mesoporous Mater.* **1999**, *33*, 197–207.
[28] T. M. Reincket, M. E. Davis, *Mater. Res. Soc. Symp. Proc.* **2002**, *724*, 209–214.
[29] N. Koumura, H. Matsumoto, H. Kawanami, N. Tamaoki, M. Yoshida, *Polym. J.* **2010**, *42*, 759–765.
[30] E. Berwig, V. L. S. Severgnini, M. S. Soldi, G. Bianco, E. A. Pinheiro, A. T. N. Pires, V. Soldi, *Polym. Degrad. Stabil.* **2003**, *79*, 93–98.
[31] S. K. Kundu, M. Yoshida, M. Shibayama, *J. Phys. Chem. B* **2010**, *114*, 1541–1547.
[32] M. Yoshida, N. Koumura, Y. Misawa, N. Tamaoki, H. Matsumoto, H. Kawanami, S. Kazaoui, N. Minami, *J. Am. Chem. Soc.* **2007**, *129*, 11039–11041.
[33] J. D. Tovar, *Acc. Chem. Res.* **2013**, *46*, 1527–1537.
[34] D. M. Guldi, N. Martín, *Carbon nanotubes and related structures. Synthesis, characterization, functionalization, and applications* Wiley-VCH, Weinheim, Germany **2010**.
[35] S. Taruta, M. Endo, *Chem. Soc. Rev.* **2009**, *38*, 1897–1903.
[36] J. Bachl, T. Huber, D. Kühbeck, E.-M. Schön, G. Brunner, B. Kraus, J. Heilmann, J. A. Codelli, C. R. Bertozzi, C. Cativiela, D. D. Díaz, *Nanosci. Nanotechnol. Asia* **2012**, *2*, 200–209, and references therein.
[37] P. Angelikopoulos, H. Bock, *Phys. Chem. Chem. Phys.* **2012**, *14*, 9546–9557, and references therein.
[38] V. A. Sinani, M. K. Gheith, A. A. Yaroslavov, A. A. Rakhnyanskaya, K. Sun, A. A. Mamedov, J. P. Wicksted, N. A. Kotov, *J. Am. Chem. Soc.* **2005**, *127*, 3463–3472.
[39] T. Fujinaga, N. Nakashima, *Polym. J.* **2008**, *40*, 577–589.
[40] G. Romero, S. E. Moya, *Soft Matter* **2012**, *8*, 9727–9730, and references therein.
[41] Z. Wang, Y. Chen, *Macromolecules* **2007**, *40*, 3402–3407.
[42] X. Tong, J. Zheng, Y. Lu, Z. Zhang, H. Cheng, *Mater. Lett.* **2007**, *61*, 1704–1706, and references therein.
[43] M. Asai, K. Sugiyasu, N. Fujita, S. Shinkai, *Chem. Lett.* **2004**, *33*, 120–121.
[44] R. Shvartzman-Cohen, Y. Levi-Kalisman, E. Nativ-Roth, R. Yerushalmi-Rozen, *Langmuir* **2004**, *20*, 6085–6088.
[45] R. Allen, Z. Bao, G. G. Fuller, *Nanotechnology* **2013**, *24*, 015709.
[46] S. K. Kundu, T. Matsunaga, M. Yoshida, M. Shibayama, *J. Phys. Chem. B* **2008**, *112*, 11537–11541.
[47] S. Bartoli, S. Roelens, *J. Am. Chem. Soc.* **2002**, *124*, 8307–8315.
[48] D.-X. Wang, M.-X. Wang, *J. Am. Chem. Soc.* **2013**, *135*, 892–897.
[49] P. Ballester, *Acc. Chem. Res.* **2013**, *46*, 874–884.